Quantum Phases of Three-Dimensional Chiral Topological Insulators on a Spin Quantum Simulator

Tao Xin,[*] Yishan Li, Yu-ang Fan, Xuanran Zhu⬤, Yingjie Zhang, Xinfang Nie, Jun Li,[†] Qihang Liu,[‡] and Dawei Lu⬤[§]

Shenzhen Institute for Quantum Science and Engineering and Department of Physics, Southern University of Science and Technology, Shenzhen 518055, China

The detection of topological phases of matter has become a central issue in recent years. Conventionally, the realization of a specific topological phase in condensed matter physics relies on probing the underlying surface band dispersion or quantum transport signature of a real material, which may be imperfect or even absent. On the other hand, quantum simulation offers an alternative approach to directly measure the topological invariant on a universal quantum computer. However, experimentally demonstrating high-dimensional topological phases remains a challenge due to the technical limitations of current experimental platforms. Here, we investigate the three-dimensional topological insulators in the AIII (chiral unitary) symmetry class, which yet lack experimental realization. Using the nuclear magnetic resonance system, we experimentally demonstrate their topological properties, where a dynamical quenching approach is adopted and the dynamical bulk-boundary correspondence in the momentum space is observed. As a result, the topological invariants are measured with high precision on the band-inversion surface, exhibiting robustness to the decoherence effect. Our Letter paves the way toward the quantum simulation of topological phases of matter in higher dimensions and more complex systems through controllable quantum phases transitions.

Introduction.—The past decades have witnessed a new era of condensed matter physics after the milestone discovery of the quantum Hall [1,2], quantum spin Hall [3–5], and quantum anomalous Hall effect [6–9] that established the link between topology and electronic structure. Topological insulators, in general, are such fermionic phases with a gapped n-dimensional (nD) bulk state but gapless $(n-1)$D boundary states protected by the generic symmetries of the Hamiltonian [4,5,10–15]. Considering time-reversal symmetry, particle-hole symmetry, and their combination, chiral symmetry, there are ten topological classes within the framework of Altland-Zirnbauer classification [16,17]. While the central physics of the topological nature can be sketched within a few energy bands, such a clean picture at the Fermi level in condensed matter systems is extremely difficult to realize. This is because the huge amount of electrons in complex materials leads to dense manifold of states as a visual effect, named band spaghetti [18], not to mention other detrimental factors such as impurities and domains. As a result, although the topological insulators of A [2D Cr doped (Bi,Sb)Te] [19,20], AII (3D Bi_2Se_3) [21], and DIII class (3D B phase of ^{3}He) [22,23] have been experimentally confirmed, several topological classes, e.g., 2D chiral p-wave (D class) and d-wave topological superconductors (C class), are still in controversy among various material candidates, such as Sr_2RuO_4 [24,25], SrPtAs [26,27], and URu_2Si_2 [28,29], etc. More importantly, there are still a number of topological classes waiting for realization.

Recently, quantum simulation has also demonstrated a powerful tool [30–37] to investigate topological phases accompanied with the emergence of modern quantum technologies. As the parameters of the simulator are highly controllable, it can directly work on a minimal Hamiltonian and thus get rid of the complication of real materials. At present, quantum simulation of topological systems has been carried out in cold atoms [30,36,38–41], superconducting circuits [42], and nitrogen-vacancy (NV) defects in diamond [35]. Interestingly, all of these works focused on 1D and 2D topological insulators or their derivatives. For example, the 1D AIII topological Anderson insulator has been realized in disordered atomic wires [43], the 2D quantum anomalous Hall insulator has been simulated in the ultracold ^{87}Rb gas [44], and the 3D Weyl semimetal with the same topological nature of a 2D Chern insulator has been simulated by single-qubit superconducting circuits [45]. Hence, the experimental realization of a 3D topological insulator is still lacking.

The minimum models of 1D and 2D topological insulators can be described within a two-band Hamiltonian manipulated by a single-qubit system. In contrast, the simulation of a 3D topological insulator requires at least a four-band model within in a 2-qubit system [46]. Meanwhile, the necessity of realizing 3D topological insulators also lies in the possibility for exploring more

emergent topological phenomena, such as higher-order bulk-surface correspondence [47]. Hence, in this Letter, we demonstrate for the first time quantum simulation of a 3D AIII class (chiral unitary) topological insulator in a nuclear magnetic resonance (NMR) quantum simulator. Such a topological class only respects chiral symmetry, without any counterparts in condensed matter physics yet. Zhang *et al.* [48–50] proposed a dynamical quench approach to uncover topology and bulk-boundary correspondence for high-dimensional topological phases. One measures the time-averaged spin texture on the nodes of band inversion when turning off the spin-orbit coupling, i.e., band-inversion surface (BIS), via quenching the Hamiltonian of the system in the topological region. In particular, a 3D topological phase can be encoded into a 2D subregion to reduce the complexity of characterizing topological patterns in experiment.

3D AIII model.—In this Letter, we realize the 3D AIII class topological insulator with the Hamiltonian

$$\mathcal{H}(\mathbf{k}) = h_0 \sigma_z^1 \sigma_x^2 + h_1 \sigma_x^1 + h_2 \sigma_y^1 + h_3 \sigma_z^1 \sigma_z^2. \tag{1}$$

Here, $h_0 = m_z - \xi_0(\cos k_x + \cos k_y + \cos k_z)$ characterizes the dispersion of the decoupled bands, while $h_1 = \xi_{SO} \sin k_x$, $h_2 = \xi_{SO} \sin k_y$, and $h_3 = \xi_{SO} \sin k_z$ denote the spin-orbit (SO) field. In this model, $h_0(\mathbf{k}) = 0$ in the momentum space defines the BIS. Figure 1(a) presents a band structure of a 3D topological insulator.
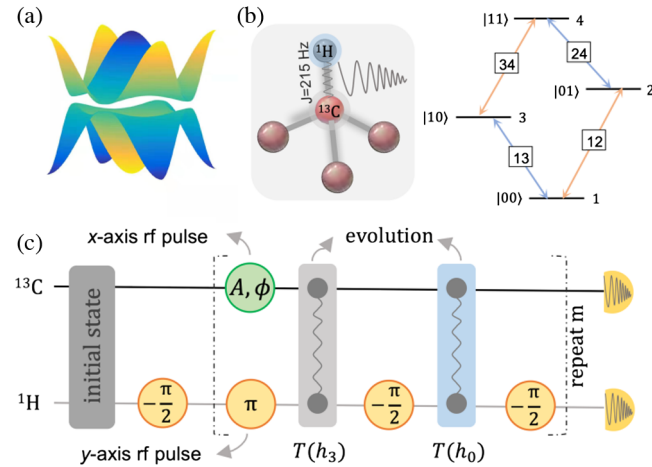

FIG. 1. (a) Band structure of a 3D topological insulator with the Hamiltonian $\mathcal{H}(\mathbf{k})$ when $m_z = 0.86\xi_0$ and $k_z = \pi/6$. (b) Molecular structure of ^{13}C-labeled chloroform with the coupling $J = 215$ Hz and the splitting energy levels under a magnetic field. (c) Pulse sequence using the Trotter approximation to simulate the topological Hamiltonian $\mathcal{H}(\mathbf{k})$ when $h_0 < 0$ and $h_3 < 0$. The green circle represents a rotation around the x axis with the pulse amplitude A and the phase ϕ. The orange circles represent the y-axis rotations with the displaying angles. The gray and blue blocks are the free evolutions under the J-coupling Hamiltonian with the evolution time $T(h_3) = (2|h_3|/\pi J)\tau$ and $T(h_0) = (2|h_0|/\pi J)\tau$, respectively.

Both of the valence band and the conduction band are doubly degenerate due to the chiral symmetry. According to the classification theory at equilibrium, the 3D topological phases of this model include three nontrivial areas dictated by m_z: (i) winding number $\nu_3 = 2$ when $|m_z| < \xi_0$; (ii) $\nu_3 = -1$ when $\xi_0 < m_z < 3\xi_0$; and (iii) $\nu_3 = -1$ when $-3\xi_0 < m_z < -\xi_0$. The region with $|m_z| > 3\xi_0$ has only trivial phases.

In nonequilibrium classification, the topological invariant of $\mathcal{H}(\mathbf{k})$ described by the 3D winding number can be determined in a dynamical quench process. At $t < 0$, the system stays in the ground state ρ_0 of the prequench $\mathcal{H}(\mathbf{k})$ with $m_z \gg \xi_0$, and then starts to evolve under the postquench $\mathcal{H}(\mathbf{k})$ by suddenly changing m_z to a nontrivial value. Denoting the spin texture by γ_i (here $\gamma_1 = \sigma_x^1$, $\gamma_2 = \sigma_y^1$, and $\gamma_3 = \sigma_z^1 \sigma_z^2$), its expectation value under a given evolution time t is thus

$$\langle \gamma_i(\mathbf{k}, t) \rangle = \text{Tr}(\gamma_i e^{-i\mathcal{H}(\mathbf{k})t} \rho_0 e^{i\mathcal{H}(\mathbf{k})t}). \tag{2}$$

On the BIS, the time-averaged spin texture $\overline{\langle \gamma_i(\mathbf{k}) \rangle}$ vanishes, so it can be employed to characterize the quench dynamics. However, to determine the topological invariant requires more effort, in that the difference of $\overline{\langle \gamma_i(\mathbf{k}) \rangle}$ across the BIS needs to be acquired. This parameter is quantified by a dynamical spin-texture field $g_i(\mathbf{k}) = -\partial\overline{\langle \gamma_i(\mathbf{k}) \rangle}/\mathbb{N}_k \partial k_\perp$, where $\mathbb{N}_k$ is a normalization coefficient and $k_\perp$ is the direction perpendicular to the BIS from the inside out. This $\vec{g}(\mathbf{k})$ uniquely determines the contour of the topological patterns, leading to the direct acquisition of the 3D winding number.

Concisely, to detect the topological phases in experiment using the quench process, one needs to first locate the BIS and, consequently, measure the dynamical spin-texture field perpendicular to the BIS. In the following, we describe our experiment of detecting the topological number in the 3D AIII topological insulators in detail.

Experimental settings.—The demonstration is performed on the NMR. The sample is the ^{13}C-labeled chloroform dissolved in acetone-*d*6 as shown in Fig. 1(b). The ^{13}C and ^{1}H spin are used as two qubits, where each qubit can be controlled by radio-frequency (rf) fields, respectively. The total Hamiltonian is

$$\mathcal{H}_{NMR} = \frac{\pi J}{2} \sigma_z^1 \sigma_z^2 + \sum_{i=1}^{2} \pi B_i (\cos \phi_i \sigma_x^i + \sin \phi_i \sigma_y^i), \tag{3}$$

where $J = 215$ Hz is the coupling strength between qubits, and B_i and ϕ_i are tunable parameters (amplitude and phase) of the rf field. All experiments are carried out on a Bruker AVANCE 600 MHz spectrometer at 298 K.

The key concept in quantum simulation is to map the experimental Hamiltonian in Eq. (3) to the problem Hamiltonian in Eq. (1), i.e., $\mathcal{H}_{NMR} \rightarrow \mathcal{H}(\mathbf{k})$. Here, we adopt the Trotter-Suzuki formula [51,52] by decomposing

the desired Hamiltonian dynamics into repeated evolutions of elementary Hamiltonians. In regard to the problem Hamiltonian in Eq. (1), the evolution can be approximated by

$$U = e^{-i\mathcal{H}(\mathbf{k})T} \approx (e^{-i\mathcal{H}_{zx}\tau}e^{-i\mathcal{H}_{zz}\tau}e^{-i\mathcal{H}_{x,y}\tau})^m, \quad (4)$$

where $\mathcal{H}_{zx} = h_0\sigma_z^1\sigma_x^2$, $\mathcal{H}_{zz} = h_3\sigma_z^1\sigma_z^2$, $\mathcal{H}_{x,y} = h_1\sigma_x^1 + h_2\sigma_y^1$, T is the evolving time, and $m = T/\tau$ is the Trotter number. The value of m determines the precision of the approximation result. In NMR, each term on the right-hand side of Eq. (4) can be faithfully realized: $\mathcal{H}_{zx}$ and $\mathcal{H}_{zz}$ using the J-coupling evolution plus single-qubit rotations and $\mathcal{H}_{x,y}$ using a hard rf pulse acting on the first qubit. Figure 1(c) presents a NMR pulse sequence to realize the simulation of $\mathcal{H}(\mathbf{k})$ when $h_0 < 0$ and $h_3 < 0$.

Overall, the entire experiment to simulate the topological phases of the AIII class model in Eq. (1) includes four steps. (1) Prepare the ground state of the prequench Hamiltonian $\mathcal{H}(\mathbf{k})$ with $m_z \gg |\xi_0|$. We choose it as positive infinity, so the corresponding ground state is simply $(|00\rangle - |01\rangle)/\sqrt{2}$. In NMR, it is prepared by creating a (pseudo) pure state $|00\rangle$ and then applying a $-(\pi/2)$ rotation about the y axis on the second qubit. (2) Quench m_z from positive infinity, which produces a trivial phase to $m_z < |3\xi_0|$, which leads to a nontrivial topological phase. We experimentally realize this quench dynamics using the Trotter approximation in Eq. (4). (3) Measure the time-averaged spin texture $\overline{\langle\gamma_i\rangle}$ to obtain the BIS where $h_0(\mathbf{k}) = 0$. (4) Detect the dynamical spin-texture field $\vec{g}(\mathbf{k})$ according to the slope of $\overline{\langle\gamma_i\rangle}$ across the BIS. These expectation values are directly measured using standard NMR readout pulses, and the topological number of the phase can be uniquely determined by the topological patterns of $\vec{g}(\mathbf{k})$ on the BIS.

Here, we experimentally show that all three nontrivial topological phases can be detected at nonequilibrium using the quench dynamics approach, demonstrating the bulk-boundary correspondence. In experiment, the Hamiltonian in Eq. (1) is chosen as $\xi_0 = 4\xi_{SO}$ with $\xi_{SO} = 400$. The evolution time T after quenching m_z ranges from 0.5 to 5 ms with an increment 0.5 ms, meaning 10 points for each time-averaged measurement. During the Trotter approximation in Eq. (4), we fix the time slice $\tau = 0.25$ ms, so the corresponding Trotter number $m = T/\tau$ ranges from 2 to 20. Above are all of the basic parameters for our NMR quantum simulation experiment.

Locating the BIS.—Next is to locate the BIS by measuring $\overline{\langle\gamma_i\rangle}$ in the momentum space, which satisfies $h_0 = m_z - \xi_0(\cos k_x + \cos k_y + \cos k_z) = 0$. For simplicity and better visualization, we fix $k_z = \pi/6$ and discretize $k_x, k_y \in [-\pi, \pi]$ into a 24×24 lattice. Actually, this is a 2D slice (call it S) out of the entire 3D momentum space, in which we draw the topological pattern by measuring the time-averaged spin texture $\overline{\langle\gamma_i\rangle}$. The Hamiltonian $\mathcal{H}(\mathbf{k})$ is
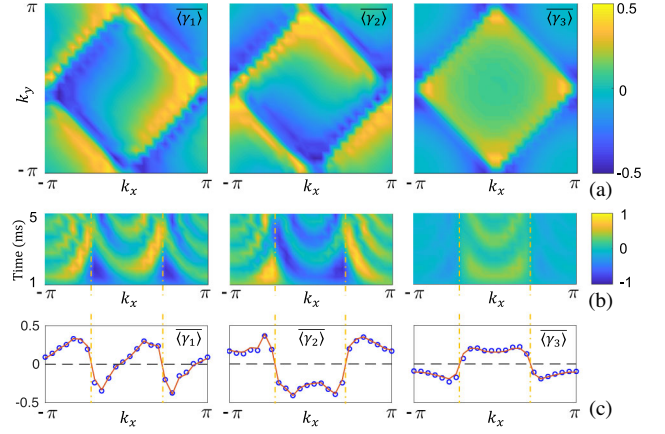

FIG. 2. Experimental BIS when quenching m_z from $m_z \gg \xi_0$ to $m_z = 0.86\xi_0$. (a) Time-averaged spin textures for different $\overline{\langle\gamma_i\rangle}$ in a 2D slice of the 3D momentum space by fixing $k_z = \pi/6$. For all γ_i's, the characterized BIS is a diamondlike pattern. (b)–(c) One typical example of how to obtain the time-averaged spin texture, corresponding to the cross section where $k_y = -\pi/2$ in (a). (b) Experimental data of the expectation values of $\langle\gamma_i\rangle$ for different evolution time $T \in [0.5, 5]$ (unit: milliseconds) with respect to k_x, while (c) shows the time-averaged results where the circles are experimental data and the solid curve is the theory.

quenched along z axis with the parameter m_z from $m_z \gg \xi_0$ to $m_z = 0.86\xi_0$. As shown in Fig. 2(a), the experimental reconstruction of $\overline{\langle\gamma_i\rangle}$ in the slice S clearly illustrates that there is a square topological pattern, which is an intersection between the BIS and S. This pattern corresponds to a 3D topological phase with the winding number $\nu_3 = 2$. To obtain the BIS in Fig. 2(a), we first measure the spin texture $\langle\gamma_i\rangle$ as a function of the evolution time T with $T \in [0.5, 5]$ in the unit of milliseconds, and then calculate its time average. Figure 2(b) shows a typical example of the value of $\langle\gamma_i\rangle$ with respect to k_x when $k_y = -\pi/2$ and $k_z = \pi/6$. Figure 2(c) shows the time-averaged spin texture $\overline{\langle\gamma_i\rangle}$ in the setting of Fig. 2(b), which is clearly a perfect match with the theoretical prediction.

Measuring the winding number.—After locating the BIS, we detect the dynamical spin-texture field $\vec{g}(\mathbf{k})$ according to the slope of $\overline{\langle\gamma_i\rangle}$ across the BIS. As the AIII class model described by Eq. (1) implies three nontrivial topological phases, we elaborate on the results of the three cases, respectively.

Case I: $|m_z| < \xi_0$: We quench the Hamiltonian $\mathcal{H}(\mathbf{k})$ along the z axis from a trivial phase to a nontrivial phase with $m_z = 0$. We choose two surfaces near the BIS that $S_- : h_0 = -0.1\xi_0$ and $S_+ : h_0 = 0.1\xi_0$ to measure the time-averaged spin operators $\langle\gamma_i\rangle$, where on each surface a total number of 195 points are sampled. Figure 3(a) presents the measured values of $\overline{\langle\gamma_i\rangle}$ for S_- and S_+, apparently displaying that the sign of the values on these two surfaces are opposite. The dynamical spin-texture field $\vec{g}(\mathbf{k})$ is hence computed from the differences of $\overline{\langle\gamma_i\rangle}$ between two
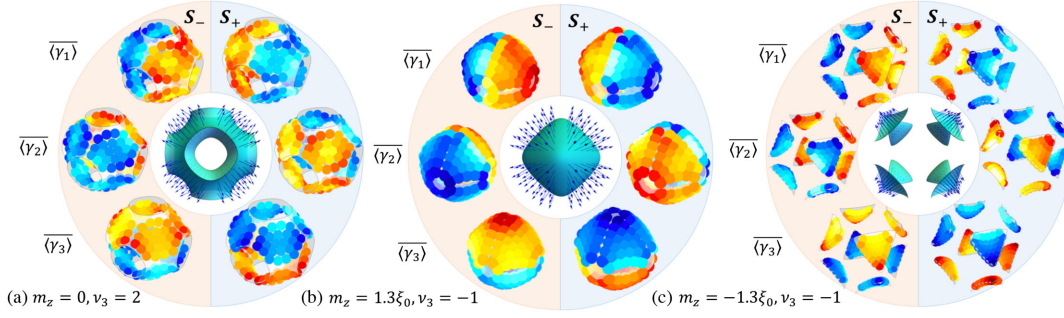
FIG. 3. (a)–(c) Measured time-averaged spin textures $\overline{\langle\gamma_i\rangle}$ on the two surfaces S_- and S_+ for the three nontrivial topological phases in the momentum space ($k_x, k_y, k_z \in [-\pi, \pi]$), respectively. The signs of $\overline{\langle\gamma_i\rangle}$ are reversed on the two surfaces across the BIS, which are used to compute the dynamical spin-texture field $\vec{g}(\mathbf{k})$. The color bar ranges from -0.5 (blue) to 0.5 (red). The center subfigures are $\vec{g}(\mathbf{k})$ across the BIS ($h_0 = 0$) for the three nontrivial topological phases. These values are determined by computing the variation of the values $\overline{\langle\gamma_i\rangle}$ at the two surfaces S_- and S_+.

surfaces, where the result is shown in the center of Fig. 3(a). The pattern of $\vec{g}(\mathbf{k})$ corresponds to a winding number $\nu_3 = 2$, demonstrating that the topological feature of the 3D AIII class model can be detected via the dynamics at the BIS, i.e., the bulk-boundary correspondence.

Case II: $\xi_0 < m_z < 3\xi_0$: We quench the parameter m_z from a trivial phase to a nontrivial phase with $m_z = 1.3\xi_0$. The two surfaces near the BIS are also chosen as S_- and S_+ to be consistent with case I. Figure 3(b) presents the measured values of $\overline{\langle\gamma_i\rangle}$ on these two surfaces. Obviously, the sign is flipped when $\overline{\langle\gamma_i\rangle}$ passes through the BIS from the inside out. To determine the topological number, we measure the dynamical spin-texture field $\vec{g}(\mathbf{k})$ at the BIS by computing by the differences of $\overline{\langle\gamma_i\rangle}$ between the two surfaces. The center of Fig. 3(b) presents the direction of $\vec{g}(\mathbf{k})$ across the BIS, whose pattern corresponds to a 3D topological phase with the winding number $\nu_3 = -1$.

Case III: $-3\xi_0 < m_z < -\xi_0$: This case is equivalent to case II with the same winding number $\nu_3 = -1$, while manifesting a closed BIS centered at the corner of the Brillouin zone. We quench the parameter to $m_z = -1.3\xi_0$, with the spin textures in Fig. 3(c) and $\vec{g}(\mathbf{k})$ in the center of Fig. 3(c).

To experimentally determine an approximate value of the topological invariant, one can count the number of circles and $\vec{g}(\mathbf{k})$ directions on the BIS in the 2D case [35]. In the 3D case, the topological pattern becomes much more complex, so we choose to calculate the experimental winding number mathematically by [48]

$$\nu_3 = \frac{1}{8\pi}\sum_j \epsilon^{mnl} \int_{\mathrm{BIS}_j} d^2\mathbf{k} \cdot \hat{h}_m(\nabla\hat{h}_n \times \nabla\hat{h}_l). \quad (5)$$

Here ν_3 is the winding number of the given 3D system, ϵ^{mnl} stands for the 3D Levi-Civita symbol, $\hat{h}$ is the normalized version of vector h with m, n, and l being the three coordinates. The sum of j ensures that all components of

BIS have been included in the integral. Based on the experimental data, the calculated winding numbers for cases I–III are $\nu_3^{\mathrm{exp}} = 1.960$, -0.985, and -0.988, respectively. They agree well with the theoretical predictions where the values are $\nu_3^{\mathrm{th}} = 2$, -1, and -1, with the inaccuracies in terms of percentage as 2.0%, 1.5%, and 1.2%, respectively. Moreover, we analyze the errors from the experimental data by computing the average error for all data points. It turns out to be 0.70%, 0.28%, and 0.28% for the three cases, which is reasonable for present quantum simulation experiments. Therefore, we conclude that the winding numbers as well as the topological phases of the AIII model have been observed in experiment.

Discussion.—This experiment demonstrates that a quantum simulator with state-of-the-art control technologies can be employed to investigate topological phases in high dimensions. The quench dynamics approach offers a practical way toward detecting topological phases at nonequilibrium. Although quantum simulation of topological phases has been realized in diverse quantum systems, each experimental platform has its own advantages and drawbacks. For example, the cold-atom system is genuinely an outstanding quantum simulator, but the target problem needs to be meticulously designed as the individual control of atoms is hard [44]; the superconducting circuit is a solid-state system of rapid development and advanced controls, but it requires extremely low temperature [53]; the NV center is a solid-spin system at ambient conditions, but the scalability is challenging and its current quantum simulation lies in a few qubits level [54]; the NMR system has good controllability of up to 12-qubit quantum simulators to tackle versatile Hamiltonians, but it has lack of scalability [55,56].

There are two more issues to be resolved. (1) The quench approach requires measuring the time evolution of the spin textures, implying a relatively long evolving time and potential errors due to decoherence. As quantum processors are very vulnerable to decoherence, it is necessary to analyze whether this approach is robust against

decoherence. In our system, we give a positive answer, as, on one hand, the experiment agrees well with the theory even in the presence of decoherence, and, on the other, the numerical simulation also shows that the decoherence effect is well resisted (see Supplemental Material [57]). Similar results are discussed in Ref. [35]. (2) The scalability is also an issue. For high-dimensional topological phases, to locate the BIS can be a challenging task. In experiment, one has to, in principle, discretize the momentum space into many pixels and measure the spin texture at each pixel to eventually draw the BIS that $h_0(\mathbf{k}) = 0$. This takes huge efforts, and one possible solution is to utilize some prior knowledge that may determine the BIS roughly. At present, this issue deserves further exploration in theory.

In summary, we have simulated the 3D AIII class topological insulator using the quench dynamics approach. As the first experiment to simulate the topological insulator phases beyond 2D using quantum processors, we anticipate quantum simulation to be an alternative way to study novel topological phases that lack experimental realization in condensed matter systems. Moreover, our work paves an avenue to further explore the other unconventional 3D topological phases, e.g., DIII topological superconductor by introducing *s*-wave pairing, and study the underlying topological phase transition.

Y. L. and T. X. contributed equally to this work.

Note added.—Recently, we noticed an in-parallel experiment [58] that simulates a 3D topological insulator using the same model and method on a 2-qubit NV center quantum simulator. Reference [58] and our Letter both utilized spin quantum simulators and have achieved similar results when locating the BIS and measuring the corresponding spin-texture field. The difference is that Ref. [58] shows the symmetry protection of the 3D chiral phase, in contrast to our Letter that proposes a way to quantitatively measure the topological invariants. The main conclusions of Ref. [58] and our Letter are consistent.

*xint@sustech.edu.cn
†lij3@sustech.edu.cn
‡liuqh@sustech.edu.cn
§ludw@sustech.edu.cn

[1] K. von Klitzing, G. Dorda, and M. Pepper, Phys. Rev. Lett. **45**, 494 (1980).
[2] K. von Klitzing, Rev. Mod. Phys. **58**, 519 (1986).
[3] B. A. Bernevig and S.-C. Zhang, Phys. Rev. Lett. **96**, 106802 (2006).
[4] B. A. Bernevig, T. L. Hughes, and S.-C. Zhang, Science **314**, 1757 (2006).
[5] C. L. Kane and E. J. Mele, Phys. Rev. Lett. **95**, 226801 (2005).
[6] C.-X. Liu, X.-L. Qi, X. Dai, Z. Fang, and S.-C. Zhang, Phys. Rev. Lett. **101**, 146802 (2008).
[7] Z. Qiao, S. A. Yang, W. Feng, W.-K. Tse, J. Ding, Y. Yao, J. Wang, and Q. Niu, Phys. Rev. B **82**, 161414(R) (2010).
[8] M. Ezawa, Phys. Rev. Lett. **109**, 055502 (2012).
[9] C.-Z. Chang, J. Zhang, X. Feng, J. Shen, Z. Zhang, M. Guo, K. Li, Y. Ou, P. Wei, L.-L. Wang *et al.*, Science **340**, 167 (2013).
[10] D. J. Thouless, M. Kohmoto, M. P. Nightingale, and M. den Nijs, Phys. Rev. Lett. **49**, 405 (1982).
[11] X.-G. Wen, Adv. Phys. **44**, 405 (1995).
[12] C. L. Kane and E. J. Mele, Phys. Rev. Lett. **95**, 146802 (2005).
[13] D. Hsieh, D. Qian, L. Wray, Y. Xia, Y. S. Hor, R. J. Cava, and M. Z. Hasan, Nature (London) **452**, 970 (2008).
[14] Y. Xia, D. Qian, D. Hsieh, L. Wray, A. Pal, H. Lin, A. Bansil, D. Grauer, Y. S. Hor, R. J. Cava *et al.*, Nat. Phys. **5**, 398 (2009).
[15] L. Fu and C. L. Kane, Phys. Rev. Lett. **102**, 216403 (2009).
[16] A. Altland and M. R. Zirnbauer, Phys. Rev. B **55**, 1142 (1997).
[17] A. P. Schnyder, S. Ryu, A. Furusaki, and A. W. W. Ludwig, Phys. Rev. B **78**, 195125 (2008).
[18] K. Rossnagel and N. V. Smith, Phys. Rev. B **73**, 073106 (2006).
[19] J. Zhang, C.-Z. Chang, P. Tang, Z. Zhang, X. Feng, K. Li, L.-l. Wang, X. Chen, C. Liu, W. Duan *et al.*, Science **339**, 1582 (2013).
[20] M. Ye, W. Li, S. Zhu, Y. Takeda, Y. Saitoh, J. Wang, H. Pan, M. Nurmamat, K. Sumida, F. Ji *et al.*, Nat. Commun. **6**, 8913 (2015).
[21] D. Hsieh, Y. Xia, D. Qian, L. Wray, J. Dil, F. Meier, J. Osterwalder, L. Patthey, J. Checkelsky, N. P. Ong *et al.*, Nature (London) **460**, 1101 (2009).
[22] L. Levitin, R. Bennett, A. Casey, B. Cowan, J. Saunders, D. Drung, T. Schurig, and J. Parpia, Science **340**, 841 (2013).
[23] L. V. Levitin, B. Yager, L. Sumner, B. Cowan, A. J. Casey, J. Saunders, N. Zhelev, R. G. Bennett, and J. M. Parpia, Phys. Rev. Lett. **122**, 085301 (2019).
[24] W.-S. Wang, C.-C. Zhang, F.-C. Zhang, and Q.-H. Wang, Phys. Rev. Lett. **122**, 027002 (2019).
[25] H. Wang, J. Luo, W. Lou, J. Ortmann, Z. Mao, Y. Liu, and J. Wei, New J. Phys. **19**, 053001 (2017).
[26] J.-F. Liu, Y. Xu, and J. Wang, Sci. Rep. **7**, 43899 (2017).

[27] D. A. Mayoh, A. D. Hillier, K. Götze, D. M. Paul, G. Balakrishnan, and M. R. Lees, Phys. Rev. B **98,** 014502 (2018).

[28] H.-H. Kung, R. Baumbach, E. Bauer, V. Thorsmølle, W.-L. Zhang, K. Haule, J. Mydosh, and G. Blumberg, Science **347,** 1339 (2015).

[29] S. Kittaka, Y. Shimizu, T. Sakakibara, Y. Haga, E. Yamamoto, Y. Ōnuki, Y. Tsutsumi, T. Nomoto, H. Ikeda, and K. Machida, J. Phys. Soc. Jpn. **85,** 033704 (2016).

[30] M. Aidelsburger, M. Atala, M. Lohse, J. T. Barreiro, B. Paredes, and I. Bloch, Phys. Rev. Lett. **111,** 185301 (2013).

[31] H. Miyake, G. A. Siviloglou, C. J. Kennedy, W. C. Burton, and W. Ketterle, Phys. Rev. Lett. **111,** 185302 (2013).

[32] G. Jotzu, M. Messer, R. Desbuquois, M. Lebrat, T. Uehlinger, D. Greif, and T. Esslinger, Nature (London) **515,** 237 (2014).

[33] M. Aidelsburger, M. Lohse, C. Schweizer, M. Atala, J. T. Barreiro, S. Nascimbène, N. Cooper, I. Bloch, and N. Goldman, Nat. Phys. **11,** 162 (2015).

[34] N. Fläschner, B. Rem, M. Tarnowski, D. Vogel, D.-S. Lühmann, K. Sengstock, and C. Weitenberg, Science **352,** 1091 (2016).

[35] Y. Wang, W. Ji, Z. Chai, Y. Guo, M. Wang, X. Ye, P. Yu, L. Zhang, X. Qin, P. Wang, F. Shi, X. Rong, D. Lu, X.-J. Liu, and J. Du, Phys. Rev. A **100,** 052328 (2019).

[36] Z. Wu, L. Zhang, W. Sun, X.-T. Xu, B.-Z. Wang, S.-C. Ji, Y. Deng, S. Chen, X.-J. Liu, and J.-W. Pan, Science **354,** 83 (2016).

[37] B. Pérez-González, M. Bello, G. Platero, and A. Gómez-León, Phys. Rev. Lett. **123,** 126401 (2019).

[38] X.-J. Liu, K. T. Law, and T. K. Ng, Phys. Rev. Lett. **112,** 086401 (2014).

[39] B. Song, L. Zhang, C. He, T. F. J. Poon, E. Hajiyev, S. Zhang, X.-J. Liu, and G.-B. Jo, Sci. Adv. **4,** eaao4748 (2018).

[40] X.-J. Liu, K. T. Law, T. K. Ng, and P. A. Lee, Phys. Rev. Lett. **111,** 120402 (2013).

[41] C.-R. Yi, L. Zhang, L. Zhang, R.-H. Jiao, X.-C. Cheng, Z.-Y. Wang, X.-T. Xu, W. Sun, X.-J. Liu, S. Chen, and J.-W. Pan, Phys. Rev. Lett. **123,** 190603 (2019).

[42] E. Flurin, V. V. Ramasesh, S. Hacohen-Gourgy, L. S. Martin, N. Y. Yao, and I. Siddiqi, Phys. Rev. X **7,** 031023 (2017).

[43] E. J. Meier, F. A. An, A. Dauphin, M. Maffei, P. Massignan, T. L. Hughes, and B. Gadway, Science **362,** 929 (2018).

[44] W. Sun, C.-R. Yi, B.-Z. Wang, W.-W. Zhang, B. C. Sanders, X.-T. Xu, Z.-Y. Wang, J. Schmiedmayer, Y. Deng, X.-J. Liu, S. Chen, and J.-W. Pan, Phys. Rev. Lett. **121,** 250403 (2018).

[45] X. Tan, Y. X. Zhao, Q. Liu, G. Xue, H.-F. Yu, Z. D. Wang, and Y. Yu, Phys. Rev. Lett. **122,** 010501 (2019).

[46] A. P. Schnyder, S. Ryu, A. Furusaki, and A. W. W. Ludwig, Phys. Rev. B **78,** 195125 (2008).

[47] W. A. Benalcazar, B. A. Bernevig, and T. L. Hughes, Science **357,** 61 (2017).

[48] L. Zhang, L. Zhang, S. Niu, and X.-J. Liu, Sci. Bull. **63,** 1385 (2018).

[49] L. Zhang, L. Zhang, and X.-J. Liu, Phys. Rev. A **99,** 053606 (2019).

[50] L. Zhang, L. Zhang, and X.-J. Liu, Phys. Rev. A **100,** 063624 (2019).

[51] H. F. Trotter, Proc. Am. Math. Soc. **10,** 545 (1959).

[52] M. Suzuki, Proc. Jpn. Acad. Ser. B **69,** 161 (1993).

[53] F. Arute, K. Arya, R. Babbush, D. Bacon, J. C. Bardin, R. Barends, R. Biswas, S. Boixo, F. G. Brandao, D. A. Buell *et al.*, Nature (London) **574,** 505 (2019).

[54] Y.-N. Lu, Y.-R. Zhang, G.-Q. Liu, F. Nori, H. Fan, and X.-Y. Pan, Phys. Rev. Lett. **124,** 210502 (2020).

[55] D. Lu, K. Li, J. Li, H. Katiyar, A. J. Park, G. Feng, T. Xin, H. Li, G. Long, A. Brodutch *et al.*, npj Quantum Inf. **3,** 45 (2017).

[56] J. Li, Z. Luo, T. Xin, H. Wang, D. Kribs, D. Lu, B. Zeng, and R. Laflamme, Phys. Rev. Lett. **123,** 030502 (2019).

[57] See Supplemental Material at http://link.aps.org/supplemental/10.1103/PhysRevLett.125.090502 for numerical simulations and experimental details.

[58] W. Ji, L. Zhang, M. Wang, L. Zhang, Y. Guo, Z. Chai, X. Rong, F. Shi, X.-J. Liu, Y. Wang *et al.*, Phys. Rev. Lett. **125,** 020504 (2020).